

*Short Communication*

## **Mechanical Properties and Corrosion Behaviors of Novel Cr<sub>2</sub>Ni Low-Alloy Construction Steel**

*Hong Liu*

Civil Engineering Department, Shanxi University, Taiyuan 030013, China

E-mail: [Liuhongdz76@sohu.com](mailto:Liuhongdz76@sohu.com)

*Received:* 4 December 2014 / *Accepted:* 12 January 2015 / *Published:* 19 January 2015

---

The novel Cr<sub>2</sub>Ni low-alloy construction steel with good matched strength and toughness was developed through a reasonable thermo-mechanical control process (TMCP). Microhardness, impact toughness and tensile properties of this steel were measured and compared with a traditional X60 steel. The corrosion resistance was determined by immersion tests combined with weight loss method. The electrochemical corrosion behaviors were investigated using potentiodynamic sweeps, electrochemical impedance spectroscopy (EIS) and scanning electron microscopy (SEM). The results showed that the novel Cr<sub>2</sub>Ni steel can achieve much better mechanical properties and corrosion performance than X60 steel. Compared with traditional X60 steel, the impact energy (~ 240 J) of Cr<sub>2</sub>Ni steel increased by one time approximately. Uniform corrosion characteristic was present to the Cr<sub>2</sub>Ni steel. As a result of the protectiveness of the Cr rich film, the novel Cr<sub>2</sub>Ni steel showed much better corrosion resistance than X60 steel.

---

**Keywords:** Low-alloy construction steel; Mechanical property; Corrosion behavior; SEM; EIS

### **1. INTRODUCTION**

For carbon steels used for construction, mechanical property is of vital importance and has been studied by numerous researches [1-4]. Meanwhile, the corrosion resistance of construction steel is also becoming more and more important. An interesting research by Panasyuk [5] studied the corrosion-hydrogen degradation of the Shukhov Lattice construction steels and found that the fracture was caused by the intensive corrosion damage of the steel. For the corrosion films on that formed on traditional carbon steel used for construction, previous studies [6-9] have proposed basically the same description on the rust layer structure, which showed that the rust layer on the steel was divided into two layers and the outer layer was much loose. Generally, this kind of loose scale has a poor protectiveness for the steel substrate. Therefore, for some harsh environments, such as seaside,

corrosion resistant alloys (CRAs) such as stainless steels are often used to avoid corrosion risks. Although CRAs have good corrosion resistance, they are very expensive and thus cannot be used extensively [10].

Therefore, the newly developed Cr containing (< 5%) low-alloy steels were developed in recent years [11-13]. The Cr containing low-alloy steels can take a good balance between traditional carbon steels and CRAs in terms of cost and performance [14,15]. In this work, a 2% Cr containing low-alloy construction steel (Cr2Ni steel) with good matched strength and toughness was developed through a reasonable thermo-mechanical control process (TMCP). Mechanical properties and corrosion behaviors of this steel were measured, and a traditional X60 steel served as a contrast. The results showed that the Cr2Ni steel had much better mechanical properties and corrosion resistance than the traditional X60 steel.

## 2. EXPERIMENTAL DETAILS

The novel Cr2Ni steel was used as the experimental material and a commercial X60 steel served as comparison. Table 1 lists the main chemical composition of these two steels.

**Table 1.** Main chemical composition of Cr2Ni and X60 construction steels ( $\omega$ t, %)

Element	C	Cr	Mo	Si	Mn	Ni	S	P	Fe
Cr2Ni	0.08	1.98	0.15	0.28	0.75	0.98	0.006	0.004	Bal.
X60	0.05	-/-	0.17	0.19	1.48	-/-	0.005	0.024	Bal.

The tensile and impact properties of Cr2Ni and X60 steels were tested according to CN-GB/T 2651-2008 [16] and CN-GB/T 2650-2008 [17], respectively. The flake tensile samples of 120 mm  $\times$  18 mm  $\times$  3 mm were tested using MTS810 type universal tensile testing machine. The non-standard V-notch impact samples of 55 mm  $\times$  10 mm  $\times$  5 mm were tested using JB-300B type impact tester. The measured and standard impact absorbing energies were converted through Eq. (1). According to CN-GB/T 2654-2008 [18], hardness values of Cr2Ni and X60 steels were tested using DHV-1000Z type micro-sclerometer with a loading of 9.8 N and an enduring time of 15 s.

$$KV = \frac{8 \times 10 \times KV_m}{A} \quad (1)$$

where  $KV$  is the standard impact absorbing energy (J);  $KV_m$  is the measured value (J);  $A$  is the area of fracture ( $\text{mm}^2$ ).

The immersion tests were performed to determine the corrosion resistance of Cr2Ni and X60 steels. The corrosion rate was calculated by Eq. (2). Prior each weight loss test, the specimen was weighed using an analytical balance with an accuracy of  $10^{-4}$  g. After 7, 15, and 30 days of immersion, the corroded specimens were extracted from the solution and immediately rinsed with absolute ethyl

alcohol. The corrosion products were removed according to ASTM G1-03 standards, rinsed, dried, and reweighed to determine the final weight of the specimen.

$$C_i = \frac{87600(W_{0i} - W_{1i})}{t\rho S}; (i = 1, 2, \dots) \quad (2)$$

where  $C_i$  is the average corrosion rate, mm/y;  $W_{0i}$  and  $W_{1i}$  are the original and final weights of the specimen, g, respectively;  $t$  is the immersion time, h;  $\rho$  is the steel density, g/cm<sup>3</sup>; and  $S$  is the exposed surface area, cm<sup>2</sup>.

The surface morphology of the corrosion film on the substrate surface was observed using scanning electron microscope (SEM).

The three electrode electrochemical cell depicted in Figure 1 was used for potentiodynamic sweeps and electrochemical impedance spectroscopy (EIS) measurements. The working electrode (WE) machined from a Cr2Ni steel bulk had a 10 × 10 mm<sup>2</sup> exposed area. Before experiments, the WE was polished by silicon carbide sand paper to a 1200 grit surface finish and rinsed with deionized water, acetone and absolute ethyl alcohol successively. A platinum sheet, as a counter electrode (CE), was used in sweep and EIS tests. A saturated saturated calomel electrode (SCE) was connected to the cell via a Luggin capillary through a porous Vycor frit. The electrochemical tests were done using a potentiostat. The temperature of the electrolytes was controlled automatically within ±1°C of the preset value. The surface area of the CE was 2.25 cm<sup>2</sup>, which was much larger than the surface area of working electrode (WE).

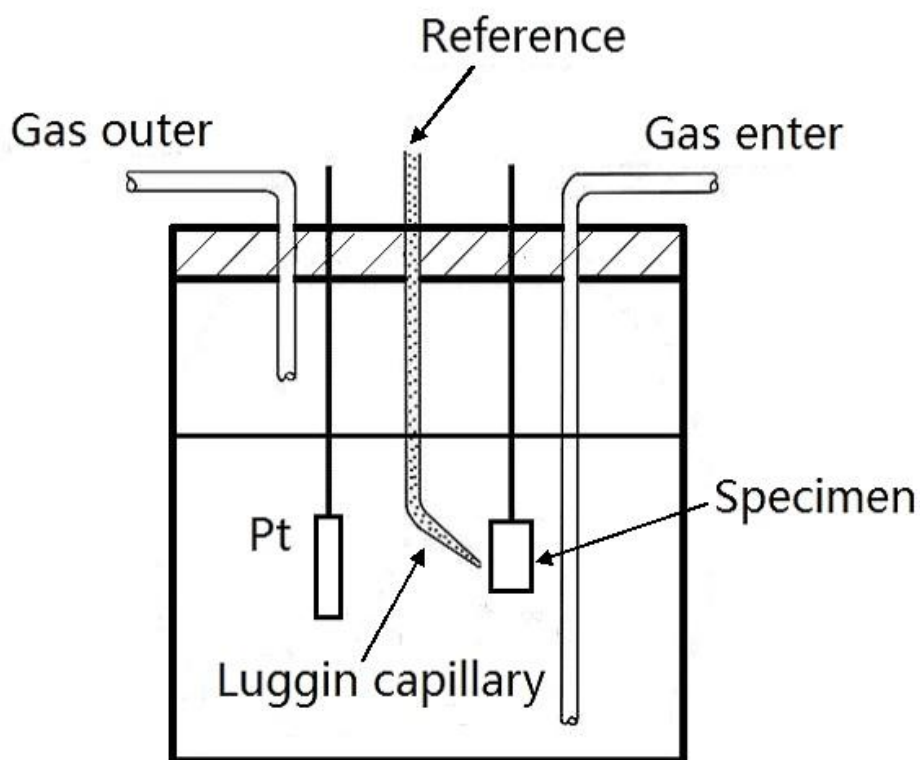


**Figure 1.** Schematic diagram showing the three electrode system used.

In potentiodynamic sweeps, the WE was polarized at  $\pm 350$  mV and the scan rate was  $0.166 \text{ mV}\cdot\text{s}^{-1}$ . The impedance spectra were recorded at different time intervals of 0, 4, 24, and 48 h using a 5 mV sinusoidal perturbing signal in the frequency range between 100 kHz and 10 mHz with eight points per decade. All the electrochemical measurements were performed using a Gamry INTERFACE 1000 electrochemical workstation.

A 1% NaCl aqueous electrolyte, which was prepared using analytical grade reagents and deionized water, was used in all tests of this work. The  $\text{N}_2$  partial pressure was 0.79 bar and the  $\text{O}_2$  partial pressure was 0.21 bar, which simulated the atmosphere. All tests conditions are summarized in Table 2.

**Table 2.** Test matrix for all electrochemical measurements

Material	Cr2Ni, X60
Solution	1 wt% NaCl
Temperature, °C	$25 \pm 1$
$\text{N}_2$ partial pressure, bar	0.79
$\text{O}_2$ partial pressure, bar	0.21
Flow	stagnant

### 3. RESULTS AND DISCUSSION

#### 3.1 Mechanical properties

Generally, the low-alloy construction steels used for earthquake resistant structure must have good matched strength and toughness. For low alloy steel, a reasonable thermo-mechanical control process (TMCP) can improve its mechanical properties well. In this section, microhardness, impact toughness and tensile properties of a novel Cr2Ni steel, which was obtained through the TMCP technique, was measured. The traditional X60 steel served as a contrast. Fig. 2 shows the hardness and impact energy values of X60 and Cr2Ni steels. Overall, Cr2Ni steel shows much higher hardness and impact energy than X60 steel. The hardness of Cr2Ni steel ( $192 \text{ HV}_{10}$ ) was 17% higher than that of X60 steel. As shown in Fig. 2b, the impact energy values of X60 steel drop quickly with the measuring temperature decreasing. By contrast, the impact energy values of Cr2Ni steel drop much more slightly, indicating that Cr2Ni steel will not exist the danger of ductile-to-brittle transition (DBT) even if the temperature reached a quite low value, such as  $-80$  °C.

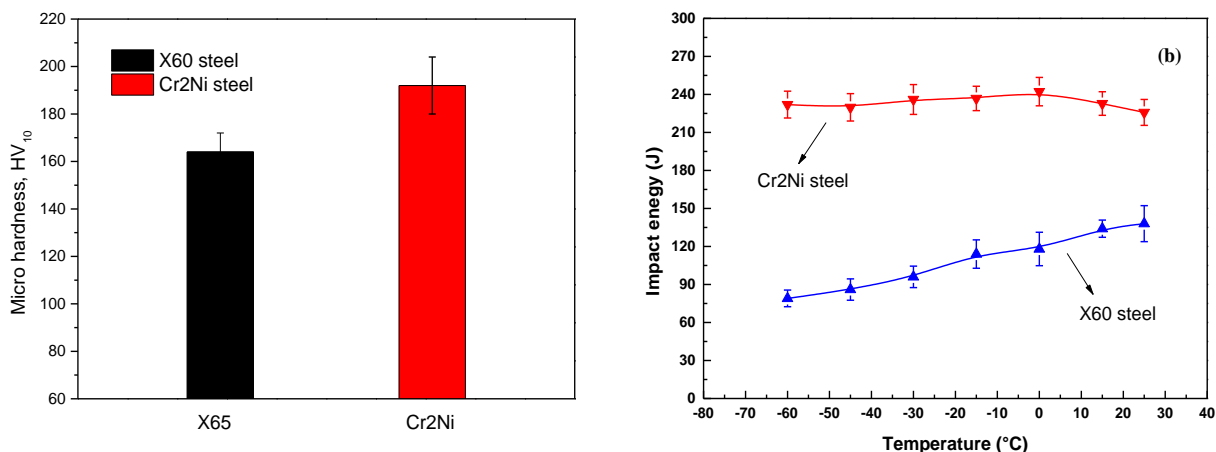


**Figure 2.** (a) Vickers hardness and (b) impact toughness values of X60 and Cr2Ni steels under different temperatures.

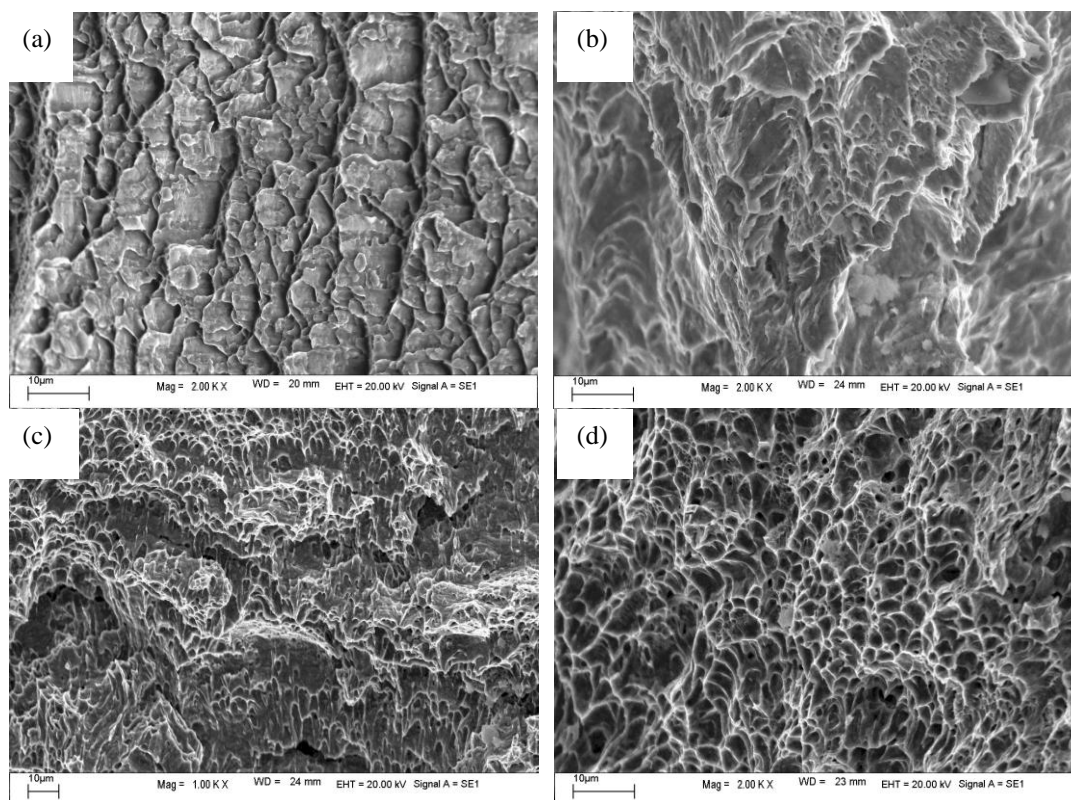


**Figure 3.** SEM photos showing the impact fracture surfaces of X60 and Cr2Ni steels under different temperatures (a) X60, -80 °C; (b) X60, 25 °C; (c) Cr2Ni, -80 °C; (d) Cr2Ni, 25 °C.

To study the mode of impact fracture of X60 and Cr2Ni steels, fractography of impact were analyzed by SEM as shown in Fig. 3a-d). At -80 °C, fracture surface of X60 steel showed a layered structure and no dimples could be seen (Fig. 3a). This kind of fracture was brittle which corresponded to the lowest impact energy [19]. Comparatively, the fracture surface of Cr2Ni steel was mainly

composed of some small and shallow dimples with a few secondary cracks (Fig. 3c). At a higher temperature of  $-25\text{ }^{\circ}\text{C}$ , the X60 steel exhibited a lot of layered ridges (Fig. 3b). However, the fracture surface of Cr2Ni steel showed numerous fine shallow and small dimples, which was ductile mode (Fig. 3d). Obviously, all these fracture characteristics in Fig. 3 were in agreement with the impact toughness values in Fig. 2b.

Table 3 gives the tensile properties of X60 and Cr2Ni steels. It can be seen that the Cr2Ni steel shows much better tensile properties than X60 steel, except in elongation. The tensile and yield strength of Cr2Ni steel reached 648 MPa and 525 MPa, which were much higher than those of X60 steel. This indicates that a reasonable TMCP technique can significantly increase the tensile properties of the low-alloy steel. Moreover, the  $R_m/R_{t0.2}$  ratio of low-alloy steel used for construction is required not below 1.2. Both the Cr2Ni and X60 steel can meet this requirement. However, the  $R_m/R_{t0.2}$  ratio of Cr2Ni steel was a little higher than that of X60 steel. In a word, the Cr2Ni steel shows better tensile properties than the traditional X60 steel.

**Table 3.** Tensile properties of X60 and Cr2Ni steels

Steel	Tensile strength $R_m$ (MPa)	Yield strength $R_{t0.2}$ (MPa)	Elongation $A_f$ (%)	Ratio $R_m/R_{t0.2}$
X60	575	475	33.5	1.21
Cr2Ni	648	525	23.2	1.23

### 3.2 Corrosion resistance and SEM morphologies

Corrosion rate is a key indicator to the evaluation of materials corrosion performance. Fig. 4 shows the corrosion rates of X60 and Cr2Ni steels after 7, 15, and 30 days immersion in our test solution. Obviously, the corrosion rates of Cr2Ni steel were much lower than those of X60 steel. With the increasing of the corrosion periods, the corrosion rates of X60 and Cr2Ni steel decreased monotonically. After 30 days immersion, the corrosion rate of Cr2Ni steel reached a very low value, which was approximately 0.16 mm/a. Moreover, the Cr2Ni steel showed a faster decreasing rate in the respect of the corrosion rate than X60 steel, indicating that the Cr2Ni steel can obtain a much better corrosion performance in a long servicing process.

Fig. 5 shows the microstructures of the corrosion films that formed on X60 and Cr2Ni steel. It can be seen that X60 steel showed a loose scale on the steel surface (Fig. 5a). Even in the denser region, it showed some big holes (Fig. 5b). By contrast, the corrosion film on Cr2Ni steel was much denser (Fig. 5c). In some areas, the film was covered by a dense crystal layer. The EDS results for the corrosion films in Fig. 5a-d are given in Table 4, respectively. As shown in Table 4, the corrosion film on X60 steel mainly consisted of O, Fe, and Mn elements.

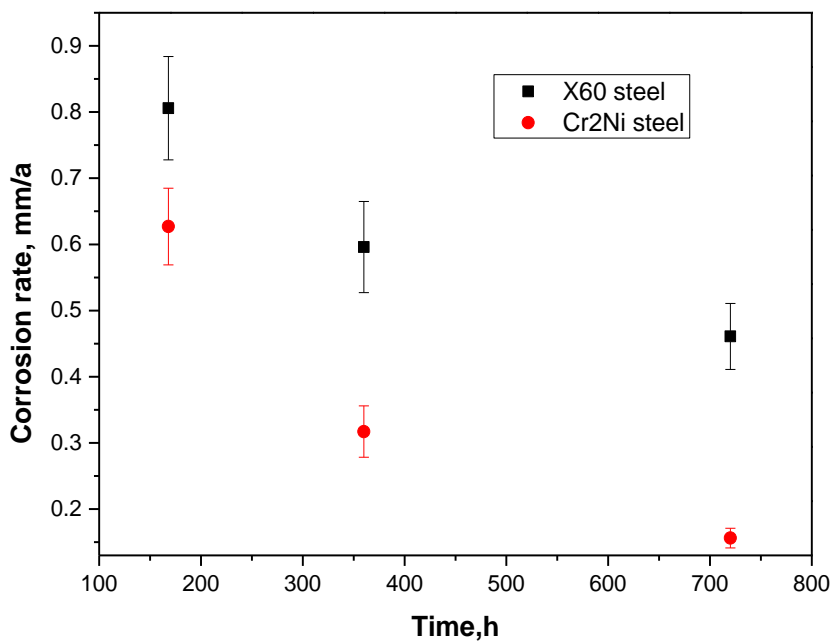


Figure 4. Corrosion rates of X60 and Cr2Ni steels after 7, 15, and 30 days immersion in test solutions.

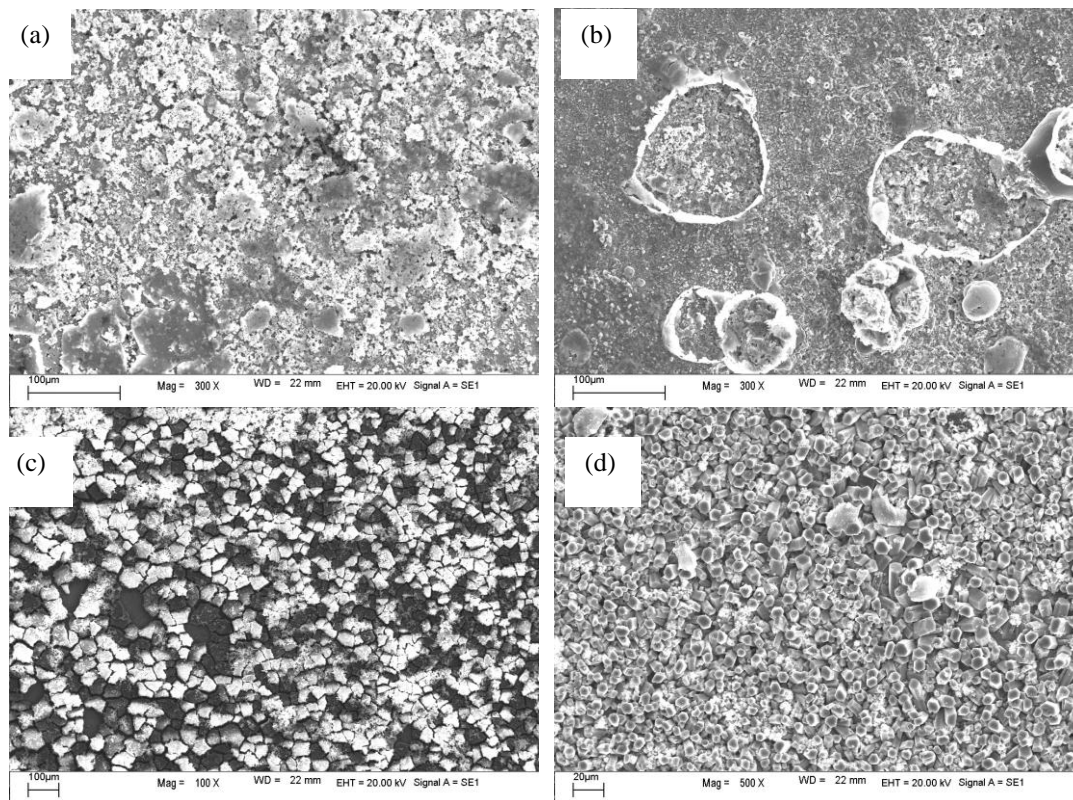


Figure 5. Microscopic morphologies of corrosion films on (a, b) X60 and (c, d) Cr2Ni samples though 30 days immersion in test solutions.

The Fe/O ratio was near to 2/3, indicating that the film was probably Fe<sub>2</sub>O<sub>3</sub>. For the holes of the corrosion film in Fig. 5b, Na and Cl were observed and Na/Cl ratio was near to 1, indicating that NaCl existed in the hole of the corrosion film on X60 steel. This salt enrichment on the corrosion film was probably the cause of the film damage. Table 4 shows that the film on Cr2Ni steel in Fig. 5c contains 17.6 wt% Cr. This Cr-enrichment film can improve the substrate corrosion resistance as a result of its effective protectiveness [20]. The EDS results of crystal layer in Fig. 5d shows that the crystal layer mainly consisted of Na and Cl. Therefore, this crystal layer was probably a NaCl layer. This salt layer was quite dense and it can protect the substrate to some extent. Above all, the film on Cr2Ni steel was much more protective than that of X60 steel. Therefore, the Cr2Ni steel shows a much lower corrosion rates in Fig. 4.

**Table 4.** EDS results of the corrosion film in Fig. 5(a-d)

Position	Element	Weight %	Atomic %
corrosion film in Fig. 5(a)	O	25.09	53.89
	Mn	1.62	1.01
	Fe	73.30	45.10
corrosion film in Fig. 5(a)	O	29.00	47.02
	Na	17.16	19.36
	Cl	27.71	20.28
	Fe	26.13	13.34
corrosion film in Fig. 5(a)	O	29.38	56.87
	Na	2.06	2.78
	Cl	1.66	1.45
	Cr	17.61	11.56
	Fe	49.29	27.34
crystal layer in Fig. 5(d)	O	2.45	4.82
	Na	33.96	46.46
	Cl	55.86	44.38
	Fe	7.73	4.34

### 3.3 Potentiodynamic sweeps and EIS measurements

Fig. 6 gives the potentiodynamic polarization curves of X60 and Cr2Ni steels. As shown in this figure, the open circuit potential (OCP) for Cr2Ni steel was about -550 mV, which was much more positive than that of X60 steel (~ -680 mV). This indicates that X60 steel has a much greater corrosion tendency than the Cr2Ni steel. For the cathodic domains, the cathodic Tafel slope for Cr2Ni steel was approximately 824mV/dec while that for X60 steel was 219 mV/dec. By contrast, the polarization slope of Cr2Ni steel was much higher than that of X60 steel, indicating that the Cr2Ni steel was much harder to be cathodically polarized. Previous studies have demonstrated that cathodic reaction could control the corrosion rate of carbon steels [21,22]. Therefore, the corrosion of the Cr2Ni steel will be inhibited as a result of the higher cathodic polarization slope.

On the other hand, for the anodic domains, the anodic Tafel slope of Cr2Ni steel ( $\sim 147$  mV/dec) was close to that of X60 steel ( $\sim 140$  mV/dec). However, the anodic polarization curve for Cr2Ni steel was always on the left of that for X60 steel. That is, the current density on the Cr2Ni steel surface was much lower than that on the X60 steel surface if the two steel samples were polarized to the same potential. Moreover, the anodic current density of Cr2Ni steel was approximately  $0.48$  mA/cm<sup>2</sup>, which was much lower than that of X60 steel ( $\sim 1.85$  mA/cm<sup>2</sup>). This indicates that the Cr2Ni steel has a much better corrosion resistance than the traditional X60 steel, which is agreement with the former experimental results in Section 3.2.

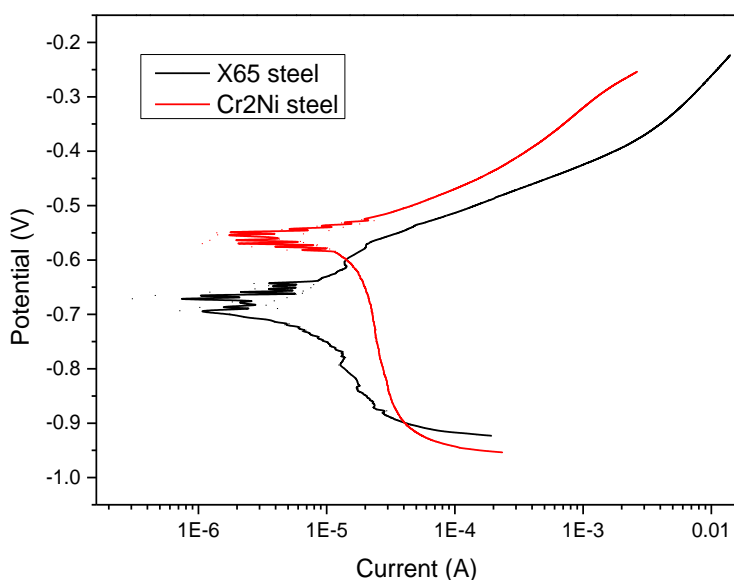


**Figure 6.** Potentiodynamic polarization curves of X60 and Cr2Ni steels.

To investigate the characteristics of the corrosion films that formed on X60 and Cr2Ni steels, the EIS measurements were performed in this section. Fig. 7 and Fig. 8 shows the Nyquist diagrams of X60 and Cr2Ni steels obtained after the immersion of 0, 4, 24, and 48 h, respectively. As shown in Fig. 7, the amplitude of the Nyquist plot increased gradually with the extension of the corrosion period, namely an outward expansion. This indicates that the X60 substrate was becoming more and more anti-corrosion. The outward expansion was mainly caused by the reduction of active regions and the growth of the corrosion films on the substrate surface. At the initial stage (0 h), a low-frequency inductive loop tended to appear in the Nyquist plot of X60 steel, which was probably related to the adsorption of the intermediate product [23]. For Cr2Ni steel, it has the similar Nyquist plots with X60 steel, showing an outward expansion (Fig. 8). However, both the amplitude and the expansion range of the Nyquist plots in Fig. 8 were much higher than those in Fig. 7. This was probably caused by two reasons: one was that the film on Cr2Ni steel surface was much more protective than that on X60 steel, the other was that the film on Cr2Ni steel grows more quickly than X60 steel. Therefore, the novel Cr2Ni steel can have such excellent corrosion resistance during a long immersion test.

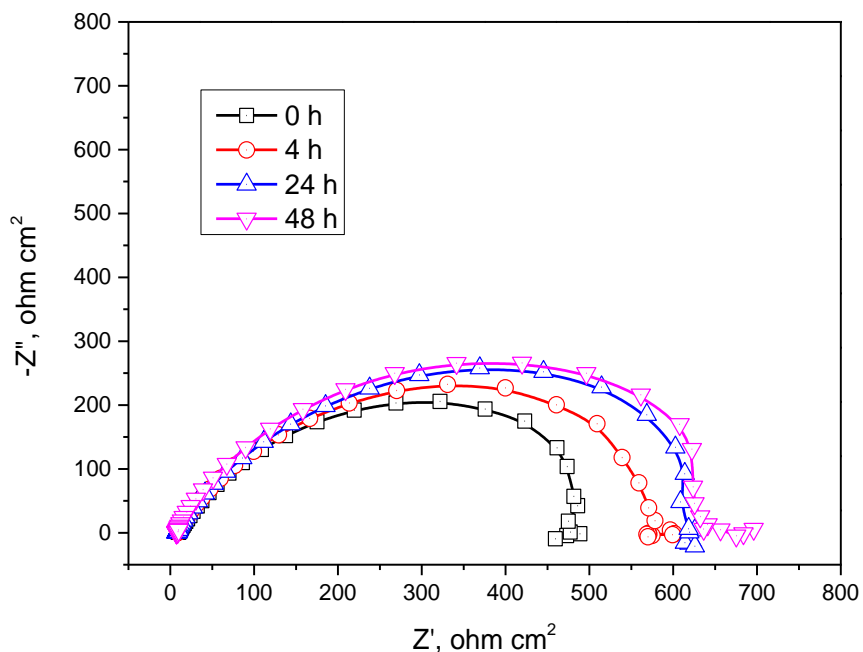


**Figure 7.** Nyquist diagrams of X60 steel obtained after the immersion of 0, 4, 24, and 48 h.

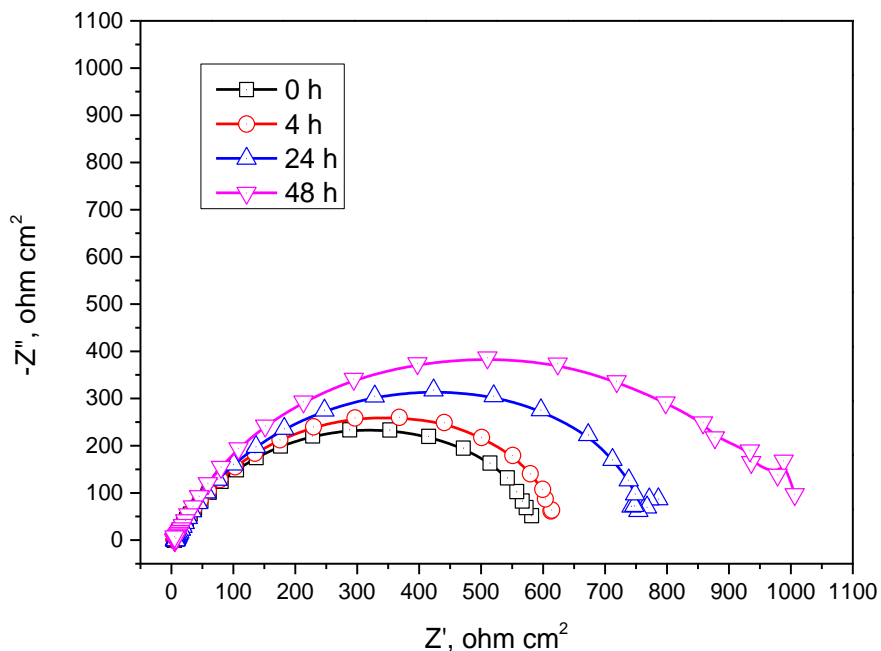


**Figure 8.** Nyquist diagrams of Cr2Ni steel obtained after the immersion of 0, 4, 24, and 48 h.

#### 4. CONCLUSION

The results obtained from this study on the mechanical properties and corrosion behaviors of the novel Cr2Ni low-alloy construction steel have been presented. The following conclusions can be drawn from this investigation:

1) The developed Cr2Ni steel shows much better mechanical properties than the traditional X60 steel. The impact energy of Cr2Ni steel reached about 240 J, which was approximately twice that of X60 steel. Tensile properties and hardness values of Cr2Ni steel were also much better than those of X60 steel.

2) The Cr2Ni steel exhibited excellent corrosion resistance with higher cathodic polarization slope, lower anodic current density and higher impedance than X60 steel. Immersion tests show that Cr2Ni steel has much lower corrosion rates as a result of a more protectiveness film than X60 steel.

## References

1. T. Yamaguchi, H. Hasegawa, K. Hagiwara, *Nippon Steel Technical Report*, 66 (1995) 17
2. C. Quchi, *ISIJ International*, 41(2001) 542
3. M. Ohashi, S. Tsuru, H. Nakao, presented at CAMP-ISIJ, Tokyo, Japan, 4 (1991) 758
4. H. Hatano, Y. Okazaki and T. Takagi, *Research and Development Kobe Steel Engineering Repots*, 53 (2002) 49
5. V. V. Panasyuk, M. Schuller, H.M. Nykyforchyn and A. I. Kutnyi, *Procedia Materials Science*, 3 (2014) 282
6. L. Caceres, T. Vargas and L. Herrsra, *Corrosion Science*, 51 (2009) 971
7. C. Q. Zhang, J. S. Wu, *Corrosion Science and Protection Technology*, 13 (2001) 143
8. J. J. Wang, X. D. Guo, *Corrosion and Protection*, 23 (2002) 288
9. T. Misawa, K. Hashimoto and S. Shimodaira, *Corrosion Science*, 14 (1974) 131
10. W. Sun, D. V. Pugh, S. Ling, R. V. Reddy and J. L. Nisbet, Shadely, *Corrosion*, 34 (2011) 647
11. L. D. Paolinelli, T. Pérez and S. N. Simison, *Materials Chemistry and Physics*, 126 (2011) 938
12. P. I. Nice, H. Takabe and M. Ueda, presented at NACE Corrosion Conference, Houston, USA, 2000, paper # 00154
13. M. B. Kermani, presented at NACE Corrosion Conference, Houston, USA, 2004, paper # 04111
14. W. W. Zhang, L. K. Ji and Q. W. Cai, *Journal of Material Engineering*, 1 (2011) 68
15. M. B. Kermani, J. C. Gonzales, C. Linne, M. Dougan and R. Cochrane, presented at NACE Corrosion Conference, Houston, USA, 2001, paper # 01065
16. CN-GB/T 2651-2008. Tensile test methods on steels. 2008
17. CN-GB/T 2650-2008. Impact test methods on steels. 2008
18. CN-GB/T 2654-2008. Hardness test methods on steels. 2008
19. J. Y. Zhu, L. N. Xu, W. Chang, L. H. Hu and M. X. Lu, *Materials and Design*, 53 (2014) 405
20. C. F. Chen, M. X. Lu, D. B. Sun, Z. H. Zhang and W. Chang, *Corrosion*, 61 (2005) 594
21. G. K. Glass, C. L. Page and N. R. Short, *Corrosion Science*, 32 (1991) 1283
22. C. H. Cao, *Electrochimica Acta*, 35 (1990) 65
23. S. Netic, *Corrosion Science*, 49 (2007) 4308